Katholieke Universiteit Leuven

Departement Elektrotechniek ESAT-SCD (SISTA) / TR 05-150

Relating the dynamics of road traffic in a stochastic cellular automaton to a macroscopic first-order model

Sven Maerivoet[†], Steven Logghe, Ben Immers, and Bart De Moor[†]

June 2005
Paper submitted for publication in
The European Physical Journal B – Condensed Matter Physics

This report is available by anonymous ftp from *ftp.esat.kuleuven.ac.be* in the directory *pub/sista/smaerivo/reports/paper-05-150.pdf*

[†]Katholieke Universiteit Leuven
Department of Electrical Engineering ESAT-SCD (SISTA)
Kasteelpark Arenberg 10, 3001 Leuven, Belgium
Phone: (+32) (0)16/32.11.46 Fax: (+32) (0)16/32.19.70
E-mail: {*sven.maerivoet,bart.demoor*}*@esat.kuleuven.ac.be*
WWW: *http://www.esat.kuleuven.ac.be/scd*
Our research is supported by: **Research Council KUL**: GOA AMBioRICS, several PhD/postdoc & fellow grants,
Flemish Government: **FWO**: PhD/postdoc grants, projects, G.0407.02 (support vector machines), G.0197.02 (power islands), G.0141.03 (identification and cryptography), G.0491.03 (control for intensive care glycemia), G.0120.03 (QIT), G.0452.04 (new quantum algorithms), G.0499.04 (statistics), G.0211.05 (Nonlinear), research communities (ICCoS, ANMMM, MLDM),
IWT: PhD Grants, GBOU (McKnow),
Belgian Federal Science Policy Office: IUAP P5/22 ('Dynamical Systems and Control: Computation, Identification and Modelling', 2002-2006), PODO-II (CP/40: TMS and Sustainability),
EU: FP5-Quprodis, ERNSI,
Contract Research/agreements: ISMC/IPCOS, Data4s,TML, Elia, LMS, Mastercard.

Please use the following BibTEX entry when referring to this document:

```
@article{MAERIVOET:05,

 author  =  "Sven Maerivoet and Steven Logghe and Ben Immers and Bart De Moor",
 title   =  "Relating the dynamics of road traffic in a stochastic
            cellular automaton to a macroscopic first-order model",
 journal =  "Submitted to The European Physical Journal B – Condensed Matter Physics"
 year    =  "2005",
 volume  =  "n/a",
 number  =  "n/a",
 pages   =  "n/a",
 month   =  jun

}
```

EPJ manuscript No.
(will be inserted by the editor)

Relating the dynamics of road traffic in a stochastic cellular automaton to a macroscopic first-order model

Sven Maerivoet[1], Steven Logghe[2], Ben Immers[3], and Bart De Moor[1]

[1] Department of Electrical Engineering ESAT-SCD (SISTA)
Katholieke Universiteit Leuven
Kasteelpark Arenberg 10, 3001 Leuven, Belgium
Phone: +32 (0)16 32 17 09 Fax: +32 (0)16 32 19 70
URL: http://www.esat.kuleuven.ac.be/scd
e-mail: sven.maerivoet@esat.kuleuven.ac.be
[2] Transport & Mobility Leuven
Vital Decosterstraat 67A bus 0001, 3000 Leuven, Belgium
Phone: +32 (0)16 31 77 30 Fax: +32 (0)16 31 77 39
URL: http://www.tmleuven.be
e-mail: steven@tmleuven.be
[3] Department of Civil Engineering Katholieke Universiteit Leuven
Kasteelpark Arenberg 40, 3001 Leuven, Belgium
Phone: +32 (0)16 32 16 69 Fax: +32 (0)16 32 19 76
URL: http://www.esat.kuleuven.ac.be/scd
e-mail: ben.immers@bwk.kuleuven.be

Received: June 28, 2005 / Revised version: June 30, 2005

Abstract. In this paper, we describe a relation between a microscopic traffic cellular automaton (TCA) model (i.e., the stochastic TCA model of Nagel and Schreckenberg) and the macroscopic first-order hydrodynamic model of Lighthill, Whitham, and Richards (LWR). The innovative aspect of our approach, is that we explicitly derive the LWR's fundamental diagram directly from the STCA's rule set, by assuming a stationarity condition that converts the STCA's rules into a set of linear inequalities. In turn, these constraints define the shape of the fundamental diagram, which is then specified to the LWR model. Application of our methodology to a simulation case study, allows us to compare the tempo-spatial behavior of both models. Our results indicate that, in the presence of noise, the capacity flows in the derived fundamental diagram are overestimations of those of the STCA model. Directly specifying the STCA's capacity flows to the LWR fundamental diagram, effectively remedies most of the mismatches between both approaches. Our methodology sees the STCA complementary to the LWR model and vice versa, so the results can be of great assistance when interpreting the traffic dynamics in both models. Especially appealing, is the fact that the STCA can visualize the higher-order characteristics of traffic stream dynamics, e.g., the fans of rarefaction waves.

PACS. 45.70.Vn Granular models of complex systems; traffic flow – 47.11.+j Computation methods in fluid dynamics – 89.40.-a Transportation

1 Introduction

Considering the existing relations between the stochastic TCA model of Nagel and Schreckenberg [16,14] and the macroscopic first-order model of Lighthill, Whitham, and Richards (LWR) [10,19], from traffic flow theory, there are already numerous links between both modeling approaches. An example is the so-called totally asymmetric simple exclusion process (TASEP) [4], which corresponds to the LWR model with a noisy and diffusive conservation law if a random sequential update is assumed [14, 15]. Another example is the STCA which can be approximated by a so-called mean field theory (MFT), and its successive refinements, such as the car-oriented mean-field theory (COMF), and the recently developed site-oriented cluster-theoretic approach [25,23,24,20,21,1,22]. A more elaborate discussion on these analytical treatments can be found in [11]. In summary, we can say that there already exist several methods for bridging both the microscopic STCA and the macroscopic LWR model (note that we do not consider the class of hybrid models, as we are only interested in direct analogies between both microscopic

and macroscopic models, and not in pure combinations of these model classes).

In this paper, we reconsider the STCA and LWR models, but we take a different approach at studying their relation: we consider a TCA model as a particle-based discretization scheme for macroscopic traffic flow models. It is from this latter point of view that our work addresses the common structure between both models. Our main goal is therefore to provide a means for implicitly incorporating the STCA's stochasticity into the LWR model, which is in fact deterministic in nature [12]. Note that we use the term *implicit* to denote the fact that the STCA's stochasticity is not introduced in the equations by means of *explicit* noise terms. Rather, our methodology implies that the stochasticity is introduced through the shape of the LWR's fundamental diagram.

This paper is organized as follows: in section 2, we briefly recapitulate both the approaches taken by traffic cellular automata models (with the STCA in particular), and the macroscopic first-order hydrodynamic LWR model. In section 3, we then consider a methodology for implicitly incorporating the STCA's stochasticity into the LWR's triangular fundamental diagram. Continuing, we apply this technique to a small case study in section 4, which points us to some discrepancies between both modeling approaches. Highlighting some of the resulting artifacts, and investigating the main reason for the difference in behavior, we move on to section 5 where we present an alternate derivation of the fundamental diagrams. Finally, the paper concludes with section 6, stating a summary of our findings.

2 Recapitulating the STCA and LWR models

With respect to the modeling of traffic flows, there are largely two model classes possible, i.e., the microscopic and macroscopic approach, respectively. In the former class, interactions between vehicles in a traffic stream are explicitly modeled, giving rise to car-following and lane-changing submodels. With respect to the latter class, traffic streams are mostly treated as inviscid but compressible fluids. In this section, we briefly recapitulate a special class of microscopic models, i.e., traffic cellular automata (TCA) models. We then describe a stochastic TCA model, called the stochastic traffic cellular automaton (STCA) of Nagel and Schreckenberg, after which we conclude with an overview of the most prominent features of the macroscopic first-order hydrodynamic model of Lighthill, Whitham, and Richards (LWR).

2.1 Traffic cellular automata (TCA) models

In the field of traffic flow modeling, microscopic traffic simulation has always been regarded as a time consuming, complex process involving detailed models that describe the behavior of individual vehicles. Approximately a decade ago, however, new microscopic models were being developed, based on the cellular automata programming paradigm from statistical physics. Let us first describe the operation of a single-lane traffic cellular automaton as depicted in Fig. 1. We assume N vehicles are driving on a circular lattice containing K cells, i.e., periodic boundary conditions (each cell can be occupied by at most one vehicle at a time). Time and space are discretized, with $\Delta T = 1$ s and $\Delta X = 7.5$ m, leading to a velocity discretization of $\Delta V = 27$ km/h. Furthermore, the velocity v_i of a vehicle i is constrained to an integer in the range $\{0, \ldots, v_{\max}\}$, with $v_{\max}$ typically 5 cells/s (corresponding to 135 km/h).

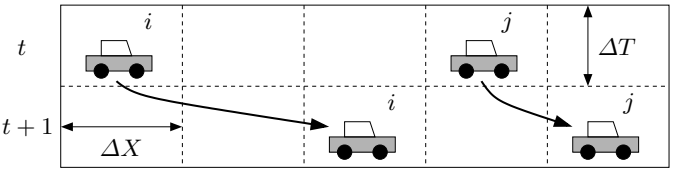

Fig. 1. Schematic diagram of the operation of a single-lane traffic cellular automaton (TCA); here, the time axis is oriented downwards, the space axis extends to the right. The TCA's configuration is shown for two consecutive time steps t and $t+1$, during which two vehicles i and j propagate through the lattice. Without loss of generality, we denote the number of empty cells in front of vehicle i as its space gap g_{s_i}.

Each vehicle i has a space headway h_{s_i} and a time headway h_{t_i}, defined as follows:

$$h_{s_i} = g_{s_i} + l_i, \tag{1}$$

$$h_{t_i} = g_{t_i} + \rho_i. \tag{2}$$

In these definitions, g_{s_i} and g_{t_i} denote the space and time gaps respectively; l_i is the length of a vehicle and ρ_i is the occupancy time of the vehicle (i.e., the time it 'spends' in one cell). Note that in a traffic cellular automaton the space headway of a vehicle is always an integer number, representing a multiple of the spatial discretization ΔX in real world measurement units. So in a jam, it is taken to be equal to the space the vehicle occupies, i.e., $h_{s_i} = 1$ cell.

Local interactions between individual vehicles in a traffic stream are modeled by means of a rule set. In this paper, we assume that all vehicles have the same physical characteristics. The system's state is changed through synchronous position updates of all the vehicles, based on a rule set that reflects the car-following behavior. Note that most rule sets of TCA models do not use the space headway h_{s_i} or the space gap g_{s_i}, but are instead based on the number of empty cells d_i in front of a vehicle i. Keeping equation (1) in mind, we therefore adopt the convention that, for a vehicle i its length $l_i = 1$ cell; the resulting TCA models are called *single-cell models*. This means that when the vehicle is residing in a compact jam, its space headway $h_{s_i} = 1$ cell and its space gap is consequently $g_{s_i} = 0$ cells. This abstraction gives us a rigorous justification to

formulate the TCA's update rules more intuitively using space gaps.

2.2 The stochastic traffic cellular automaton (STCA) model of Nagel and Schreckenberg

In 1992, Nagel and Schreckenberg proposed a TCA model that was able to reproduce several characteristics of real-life traffic flows, e.g., the spontaneous emergence of traffic jams [16,14]. Their model is called the *NaSch TCA*, but is more commonly known as the *stochastic traffic cellular automaton* (STCA). It explicitly includes a stochastic noise term in one of its rules. The STCA then comprises the following three rules (note that in Nagel and Schreckenberg's original formulation, they decoupled acceleration and braking, resulting in four rules):

R1: *acceleration and braking*

$$v_i(t) \leftarrow \min\{v_i(t-1)+1, g_{s_i}(t-1), v_{\max}\}, \quad (3)$$

R2: *randomization*

$$\xi(t) < p \Longrightarrow v_i(t) \leftarrow \max\{0, v_i(t)-1\}, \quad (4)$$

R3: *vehicle movement*

$$x_i(t) \leftarrow x_i(t-1) + v_i(t). \quad (5)$$

The STCA contains a rule for increasing the speed of a vehicle and braking to avoid collisions, i.e., rule R1, equation (3). It furthermore also contains rule R2, equation (4), which introduces stochasticity in the system. At each discrete time step t, a random number $\xi(t) \in [0,1[$ is drawn from a uniform distribution. This number is then compared with a stochastic noise parameter $p \in [0,1]$ (called the *slowdown probability*); as a result, there is a probability of p that a vehicle will slow down to $v_i(t)-1$ cells/time step. According to Nagel and Schreckenberg, the randomization of rule R2 captures natural speed fluctuations due to human behavior or varying external conditions. The rule introduces overreactions of drivers when braking, providing the key to the formation of spontaneously emerging jams. Finally, rule R3, equation (5), allows for the actual movement of vehicles in the system. The STCA model is called a *minimal model*, in the sense that all these rules are a necessity for mimicking the basic features of real-life traffic flows.

To get an intuitive feeling for the STCA's system dynamics, we have provided two time-space diagrams in Fig. 2. Both diagrams show the evolution for a global density of $k = 0.2$ vehicles/cell, but with p set to 0.1 for the left diagram, and $p = 0.5$ for the right diagram. As can be seen in both diagrams, the randomization in the model gives rise to many unstable artificial phantom mini-jams. The downstream fronts of these jams smear out, forming *unstable interfaces* [17]. This is a direct result of the fact that the intrinsic noise (as embodied by p) in the STCA model is too strong: a jam can always form at *any* density, meaning that breakdown can (and will) occur, even in the free-flow traffic regime. For low enough densities however, these jams can vanish as they are absorbed by vehicles with sufficient space headways, or by new jams in the system [8]. It has been experimentally shown that below the critical density, these jams have finite life times with a cut-off that is about 5×10^5 time steps and independent of the lattice size. When the critical density is crossed, these long-lived jams evolve into jams with an infinite life time, i.e., they will survive for an infinitely long time [13, 14,21].

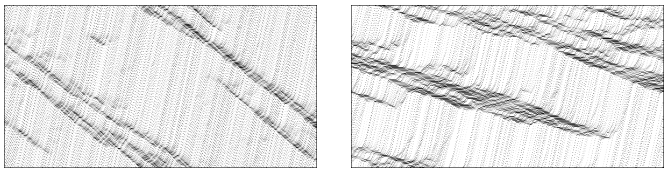

Fig. 2. Typical time-space diagrams of the STCA model (the time and space axes are oriented left to right, and bottom to top, respectively). The two shown closed-loop lattices each contain 300 cells, with a visible period of 580 time steps (each vehicle is represented as a single colored dot). Both diagrams have a global density of $k = 0.2$ vehicles/cell. *Left:* the evolution of the system for $p = 0.1$. *Right:* the evolution of the system, but now for $p = 0.5$. The effects of the randomization rule R2 are clearly visible in both diagrams, as there occur many unstable artificial phantom mini-jams. Furthermore, the speed w of the backward propagating kinematic waves decreases with an increasing p.

2.3 The macroscopic first-order traffic flow model of Lighthill, Whitham, and Richards (LWR)

Considering traffic as an inviscid but compressible fluid, it follows from this assumption, that densities k, space-mean speeds $\overline{v}_s$, and flows q are defined as continuous variables, in each point in time and space, hence leading to the names of *continuum models*, *fluid-dynamic models*, or *macroscopic models*.

The first aspect of such a fluid-dynamic description of traffic flow, consists of a *scalar conservation law*; 'scalar' because it is a first-order partial differential equation (PDE). A typical derivation can be found in [5] and [7]: the derivation is based on considering a road segment with a finite length on which no vehicles appear or disappear other than the ones that enter and exit it. After taking the infinitesimal limit, this will result in a PDE that expresses the interplay between continuous densities and flows on a local scale:

$$\frac{\partial k(t,x)}{\partial t} + \frac{\partial q(t,x)}{\partial x} = 0, \quad (6)$$

with the density k and flow q dynamically (i.e., time varying) defined over a single spatial dimension. Lighthill and Whitham were among the first to develop such a traffic flow model in 1955 [10]. One year later, Richards independently derived the same fluid-dynamic model [19],

albeit in a slightly different form. Because of the nearly simultaneous and independent development of the theory, the model has become known as the *LWR model*, after the initials of its inventors who receive the credit. In some texts, the model is also referred to as the *hydrodynamic model*, or the *kinematic wave model* (KWM), attributed to the fact that the model's solution is based on characteristics, which are called kinematic waves (e.g., shock waves).

Crucial to their approach, was a fundamental hypothesis, essentially stating that flow is a function of density, i.e., there exists a $q_e(k(t,x))$ equilibrium relationship, more commonly known as the *fundamental diagram* [6]. Central to their theory, Lighthill and Whitham assumed that the fundamental hypothesis holds at all traffic densities, not just for light-density traffic but also for congested traffic conditions.

In order to solve equation (6), we also need the *fundamental relation of traffic flow theory*, which relates the macroscopic traffic flow characteristics density k (vehicles/kilometre), space-mean speed $\overline{v}_s$ (kilometres/hour), and flow q (vehicles/hour) to each other as follows:

$$q = k\ \overline{v}_s. \tag{7}$$

In general however, there are two restrictions, i.e., the relation is only valid for (1) continuous variables, or smooth approximations of them, and (2) traffic composed of substreams (e.g., slow and fast vehicles) which comply to the following two assumptions:

Homogeneous traffic
There is a homogeneous composition of the traffic substream (i.e., the same type of vehicles).

Stationary traffic
When observing the traffic substream at different times and locations, it 'looks the same'. Putting it a bit more quantitatively, all the vehicles' trajectories in a time-space diagram should be parallel and equidistant [3].

The latter of the above two conditions, is also referred to as traffic operating in a *steady state* or at *equilibrium*. Employing the fundamental diagram $q_e(k)$, relates the two dependent variables in equation (6) to each other, thereby making it possible to solve the partial differential equation. Thus, reconsidering equation (6), taking into account the fundamental diagram, the conservation law is now expressed as:

$$k_t + q_e(k)_x = 0, \tag{8}$$

in which we introduced the standard differential calculus notation for PDEs. Recognizing the fundamental relation of traffic flow theory (7), the conservation law (8) can also be cast in a non-linear wave equation, using the chain rule for differentiation [5]:

$$k_t + \frac{dq_e(k)}{dk} k_x = 0. \tag{9}$$

Analytically solving the previous equation using the method of characteristics, results in shock waves that travel with speeds equal to:

$$w = \frac{dq_e(k)}{dk}, \tag{10}$$

i.e., the tangent to the $q_e(k)$ fundamental diagram. As a consequence, solutions, being the characteristics, of equation (9) have the following form:

$$k(t,x) = k(x - wt), \tag{11}$$

with the observation that the density is constant along such a characteristic. Whenever in the solution of the conservation equation, two of its characteristics intersect, the density takes on two different values (each one belonging to a single characteristic). As this mathematical quirk is physically impossible, the so-called entropy solution states that both characteristics terminate and breed a *shock wave*; as such, these shock waves form boundaries that discontinuously separate densities, flows, and space-mean speeds [5]. The speed of such a shock wave is related to the following ratio [18]:

$$w_{\text{shock}} = \frac{\Delta q}{\Delta k}, \tag{12}$$

with $\Delta q = q_u - q_d$ and $\Delta k = k_u - k_d$ the relative difference in flows, respectively densities, up- and downstream of the shock wave.

Note that going from a low to a high density regime typically results in a shock wave, whereas the reverse transition is accompanied by an emanation of a *fan of characteristics* (also called *expansion*, *acceleration*, or *rarefaction waves*). In shock wave theory, the densities on either side of a shock are well defined (i.e., unique solutions exist); along the shock wave however, the density jumps discontinuously from one value to another.

Because of the well-defined properties of the LWR model, it is possible to derive analytical solutions to certain types of problems. These solutions can even be drawn graphically in a time-space diagram, thereby clearly showing the evolution of first-order macroscopic traffic flow characteristics (e.g., the speed of backward-travelling jams, ...). Besides the previous analytic derivation of a solution to the conservation law expressed as a PDE, it is also possible to treat the problem numerically. Converting the PDEs into finite difference equations (FDEs), and solving them numerically stable, can be done by casting the LWR model in the context of *Godunov FDE methods*, allowing for arbitrary $q_e(k)$ fundamental diagrams [2,9]. As such, the LWR model is very appealing because it provides an attractive means for gaining insight into the primary characteristics of the evolution of traffic flows. As a surplus, the model has the benefits of the ability to efficiently construct analytical solutions, as well as the existence of thoroughly-developed and understood numerical schemes.

3 Implicitly incorporating the STCA's stochasticity

As mentioned in the introduction, we reconsider the STCA and LWR models, taking a different approach at studying their relation. Our main goal is to provide a means for implicitly incorporating the STCA's stochasticity into the LWR model. To this end, we provide a practical methodology for specifying the fundamental diagram to the LWR model. Assuming that a *stationarity condition* holds on the STCA's rules, we incorporate the STCA's stochasticity directly into the LWR's fundamental diagram.

Relating both the STCA and the LWR models is now done using a simple two-step approach, in which we first rewrite the STCA's rules into a single rule, leading to a set of *linear inequalities*. These constraints can be considered as a $\overline{v}_{s_e}(\overline{h}_s)$ fundamental diagram (see e.g., the left part in Fig. 4). This latter diagram can then be converted into an equivalent triangular flow versus density $q_e(k)$ fundamental diagram.

3.1 Rewriting the STCA's rule set

Considering a vehicle's average speed, the STCA's rules R1 and R2, equations (3) and (4) respectively, state that a vehicle slows down with probability p, and that it does not slow down with probability $1-p$. As such, they can be rewritten into the following single rule that is expressed in *continuous* speeds and space gaps:

$$\begin{aligned} v_i(t) \leftarrow p \cdot \min\{v_i(t-1) \cancel{+1} \cancel{-1}, g_{s_i}(t-1) - 1, \\ v_{\max} - 1\} + (1-p) \cdot \min\{v_i(t-1) + 1, \\ g_{s_i}(t-1), v_{\max}\}, \end{aligned} \tag{13}$$

with $v_i(t) \leftarrow \max\{0, v_i(t)\}$. Furthermore, the following two algebraic relations always hold:

$$a \cdot \min\{b, c\} = \min\{ab, ac\}, \tag{14}$$

$$\begin{aligned} \min\{a, b\} + \min\{c, d\} = \min\{a + c, a + d, \\ b + c, b + d\}. \end{aligned} \tag{15}$$

Applying relation (14) to our rule (13), yields the following result:

$$\begin{aligned} v_i(t) \leftarrow \min\{&pv_i(t-1), p(g_{s_i}(t-1) - 1), p(v_{\max} - 1)\} \\ &+\min\{(1-p)(v_i(t-1) + 1), (1-p)g_{s_i}(t-1), \\ &(1-p)v_{\max}\}. \end{aligned} \tag{16}$$

Using relation (15) to this result, allows us to obtain a formulation with a single minimum-operator:

$$\begin{aligned} v_i(t) \leftarrow \min\{\ & pv_i(t-1) + (1-p)(v_i(t-1) + 1), \\ & pv_i(t-1) + (1-p)g_{s_i}(t-1), \\ & pv_i(t-1) + (1-p)v_{\max}, \\ & p(g_{s_i}(t-1) - 1) + (1-p)(v_i(t-1) + 1), \\ & p(g_{s_i}(t-1) - 1) + (1-p)g_{s_i}(t-1), \\ & p(g_{s_i}(t-1) - 1) + (1-p)v_{\max}, \\ & p(v_{\max} - 1) + (1-p)(v_i(t-1) + 1), \\ & p(v_{\max} - 1) + (1-p)g_{s_i}(t-1), \\ & p(v_{\max} - 1) + (1-p)v_{\max}\}. \end{aligned} \tag{17}$$

Expanding all the terms between parentheses gives the following result:

$$\begin{aligned} v_i(t) \leftarrow \min\{\ & \cancel{pv_i(t-1)} + v_i(t-1) + 1 - \cancel{pv_i(t-1)} - p, \\ & pv_i(t-1) + g_{s_i}(t-1) - pg_{s_i}(t-1), \\ & pv_i(t-1) + v_{\max} - pv_{\max}, \\ & pg_{s_i}(t-1) - p + v_i(t-1) + 1 - pv_i(t-1) - p, \\ & \cancel{pg_{s_i}(t-1)} - p + g_{s_i}(t-1) - \cancel{pg_{s_i}(t-1)}, \\ & pg_{s_i}(t-1) - p + v_{\max} - pv_{\max}, \\ & pv_{\max} - p + v_i(t-1) + 1 - pv_i(t-1) - p, \\ & pv_{\max} - p + g_{s_i}(t-1) - pg_{s_i}(t-1), \\ & \cancel{pv_{\max}} - p + v_{\max} - \cancel{pv_{\max}}\}. \end{aligned} \tag{18}$$

And finally, regrouping for p yields:

$$\begin{aligned} v_i(t) \leftarrow \min\{\ & v_i(t-1) + 1 - p, \\ & p(v_i(t-1) - g_{s_i}(t-1)) + g_{s_i}(t-1), \\ & p(v_i(t-1) - v_{\max}) + v_{\max}, \\ & p(g_{s_i}(t-1) - v_i(t-1) - 2) + v_i(t-1) + 1, \\ & g_{s_i}(t-1) - p, \\ & p(g_{s_i}(t-1) - v_{\max} - 1) + v_{\max}, \\ & p(v_{\max} - v_i(t-1) - 2) + v_i(t-1) + 1, \\ & p(v_{\max} - g_{s_i}(t-1) - 1) + g_{s_i}(t-1), \\ & v_{\max} - p\}. \end{aligned} \tag{19}$$

If we now assume traffic is *stationary* (see e.g., Daganzo's description of stationary traffic in section 2.3), then we can assert that the state of a vehicle at time t is the same as its state at time $t-1$, i.e., $v_i(t) = v_i(t-1)$ and $g_{s_i}(t) = g_{s_i}(t-1)$. As a result, equation (19) gets transformed into the following set of *linear inequalities* that express constraints on the relations between $v_i(t)$, $g_{s_i}(t)$, p, and $v_{\max}$:

$$\cancel{v_i(t)} + 1 - p \geq \cancel{v_i(t)} \quad \text{(C1)},$$

$$p(v_i(t) - g_{s_i}(t)) + g_{s_i}(t) \geq v_i(t) \quad \text{(C2)},$$

$$p(v_i(t) - v_{\max}) + v_{\max} \geq v_i(t) \quad \text{(C3)},$$

$$p(g_{s_i}(t) - v_i(t) - 2) + \cancel{v_i(t)} + 1 \geq \cancel{v_i(t)} \quad \text{(C4)},$$

$$g_{s_i}(t) - p \geq v_i(t) \quad \text{(C5)},$$

$$p(g_{s_i}(t) - v_{\max} - 1) + v_{\max} \geq v_i(t) \quad \text{(C6)},$$

$$p(v_{\max} - v_i(t) - 2) + \cancel{v_i(t)} + 1 \geq \cancel{v_i(t)} \quad \text{(C7)},$$

$$p(v_{\max} - g_{s_i}(t) - 1) + g_{s_i}(t) \geq v_i(t) \quad \text{(C8)},$$

$$v_{\max} - p \geq v_i(t) \quad \text{(C9)}.$$

Let us now examine each of these nine constraints C1 through C9.

- Constraint C1 states that $1-p \geq 0$, i.e., $p \leq 1$. This logically follows from the STCA's condition that $p \in [0,1]$.
- Constraint C2 states that $p(v_i(t) - g_{s_i}(t)) + g_{s_i}(t) \geq v_i(t)$, i.e., $g_{s_i}(t)\cancel{(1-p)} \geq v_i(t)\cancel{(1-p)}$. This corresponds to $v_i(t) \leq g_{s_i}(t)$, which states that vehicles strive for collision-free driving.
- Constraint C3 states that $p(v_i(t) - v_{\max}) + v_{\max} \geq v_i(t)$, i.e., $v_{\max}\cancel{(1-p)} \geq v_i(t)\cancel{(1-p)}$. This corresponds to $v_i(t) \leq v_{\max}$, which logically follows from the STCA's condition that $v_i(t) \in \{0,\ldots,v_{\max}\}$.
- Constraint C4 states that $p(g_{s_i}(t) - v_i(t) - 2) + 1 \geq 0$, i.e., $v_i(t) \leq g_{s_i}(t) - 2 + \frac{1}{p}$ (for $p \neq 0$).
- Constraint C5 states that $g_{s_i}(t) - p \geq v_i(t)$, i.e., $v_i(t) \leq g_{s_i}(t) - p$, which is a more stringent constraint than C2 and C4.
- Constraint C6 states that $p(g_{s_i}(t) - v_{\max} - 1) + v_{\max} \geq v_i(t)$, i.e., $v_i(t) \leq v_{\max}(1-p) + p(g_{s_i}(t) - 1)$.
- Constraint C7 states that $p(v_{\max} - v_i(t) - 2) + 1 \geq 0$, i.e., $v_i(t) \leq v_{\max} - 2 + \frac{1}{p}$ (for $p \neq 0$).
- Constraint C8 states that $p(v_{\max} - g_{s_i}(t) - 1) + g_{s_i}(t) \geq v_i(t)$, i.e., $v_i(t) \leq g_{s_i}(t)(1-p) + p(v_{\max} - 1)$.
- Constraint C9 states that $v_{\max} - p \geq v_i(t)$, i.e., $v_i(t) \leq v_{\max} - p$, which is a more stringent constraint than C3 and C7.

Taking the previous considerations into account, we can see that constraints C1, C2, and C3 are always satisfied. The remaining three pairs of similar constraints on the relations between $v_i(t)$, $g_{s_i}(t)$, p, and $v_{\max}$, are the following: constraints C5 and C9, C4 and C7, and C6 and C8.

In order to gain insight into the more difficult constraints C6 and C8, we first rewrite them as follows:

$$\text{(C6)}\quad v_i(t) \leq \underbrace{p}_{\text{slope}}\, g_{s_i}(t) + \underbrace{(1-p)v_{\max} - p}_{\text{intercept}},$$

$$\text{(C8)}\quad v_i(t) \leq \underbrace{(1-p)}_{\text{slope}}\, g_{s_i}(t) + \underbrace{p(v_{\max} - 1)}_{\text{intercept}},$$

where we have separated the terms containing $g_{s_i}(t)$. Plotting the speed $v_i(t)$ versus the space gap $g_{s_i}(t)$ in Fig. 3, allows us to more easily interpret the combined effects of these two constraints. On the one hand, if we continuously change $p = 0 \rightarrow 1$, then constraint C6 goes from a horizontal line at $v_i(t) = v_{\max}$, to a slanted line with a slope of $+1$, intercepting the horizontal and vertical axes at $+1$ and -1, respectively. In all cases, the point at $(v_{\max}+1, v_{\max})$ remains invariant. On the other hand, changing $p = 0 \rightarrow 1$ turns constraint C8 from a slanted line with a slope of $+1$, passing through the origin, into a horizontal line at $v_i(t) = v_{\max} - 1$. In all cases, the point at $(v_{\max}-1, v_{\max}-1)$ remains invariant.

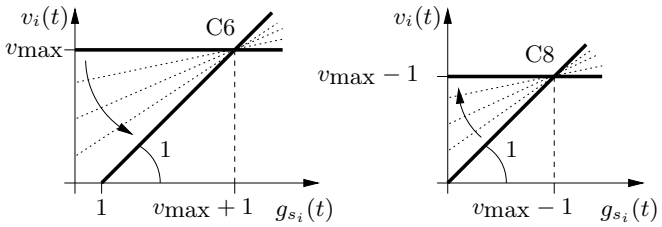

Fig. 3. A visual representation of the constraints C6 and C8. *Left:* as $p = 0 \rightarrow 1$, C6 changes from a horizontal line at $v_i(t) = v_{\max}$, to a slanted line with a slope of $+1$, intercepting the horizontal and vertical axes at $+1$ and -1, respectively. *Right:* at the same time, constraint C8 changes from a slanted line with a slope of $+1$, passing through the origin, into a horizontal line at $v_i(t) = v_{\max} - 1$.

3.2 Deriving the fundamental diagram

The next step of our approach, considers the most determining linear inequalities C5, C6, C8, and C9 as boundaries in a $\overline{v}_{s_e}(\overline{g}_s)$ fundamental diagram. As such, we note the following observations:

- **Increasing the slowdown probability p, holding $v_{\max}$ constant**:
  - The average speed $\overline{v}_{\text{ff}}$ in the free-flow regime decreases towards $v_{\max} - p$.
  - The transition point at the critical space gap g_{s_c} remains invariant.
  - The space gap g_{s_j}, corresponding to the jam density, increases.
- **Decreasing the maximum speed $v_{\max}$, holding p constant**:
  - The average speed $\overline{v}_{\text{ff}}$ in the free-flow regime decreases towards $v_{\max} - p$.
  - The transition point at the critical space gap g_{s_c} decreases.
  - The space gap g_{s_j}, corresponding to the jam density, remains invariant.

From equation (1) from traffic flow theory, it follows that a vehicle's space headway h_s is equal to its space gap g_s (i.e., the distance between the vehicle's frontal bumper and the one of its direct frontal leader), plus the vehicle's own length l. As such, the derived $\overline{v}_{s_e}(\overline{g}_s)$ fundamental diagram can be converted into a $\overline{v}_{s_e}(\overline{h}_s)$ fundamental diagram. Because we originally started from a single-cell TCA model (i.e., the STCA model with all vehicles having the same unit length), we can use our convention which states that a vehicle's length $l_i \geq 1$ cell $\propto \Delta X$ (see our discussion at the end of section 2.1 for more details).

Let us now consider the relation between the macroscopic traffic flow characteristic density k and the microscopic characteristic average space headway $\overline{h}_s$, i.e., $\overline{h}_s = k^{-1}$ [26,3]. This allows us to effectively transform the $\overline{v}_{s_e}(\overline{h}_s)$ fundamental diagram into a $\overline{v}_{s_e}(k)$ fundamental diagram. As can be seen in the left part of Fig. 4, increasing the stochasticity leads to the same observations that we previously mentioned. Finally, using the fundamental relation of traffic flow theory (7) (see section 2.3),

our constraints are transformed into an equivalent *triangular* $q_e(k)$ fundamental diagram. Applying this technique results in the following analytical expressions for the parameters of the LWR's fundamental diagram:

$$\overline{v}_{\text{ff}} = (v_{\text{max}} - p)\ \frac{\Delta X}{\Delta T}\ 3.6, \tag{20}$$

$$k_{\text{crit}} = \frac{1000}{(v_{\text{max}} + l)\ \Delta X}, \tag{21}$$

$$k_{\text{jam}} = \frac{1000}{(l + p)\ \Delta X}, \tag{22}$$

with $l = 1$ cell as the length of all vehicles in the single-cell STCA model. The capacity flow is calculated using the fundamental relation (7), resulting in the following expression:

$$q_{\text{cap}} = k_{\text{crit}}\ \overline{v}_{\text{ff}}. \tag{23}$$

As is visible in the right part of Fig. 4, an increase of the stochasticity leads to a lower capacity flow q_{cap}, an invariant critical density k_c, and a smaller jam density k_j.

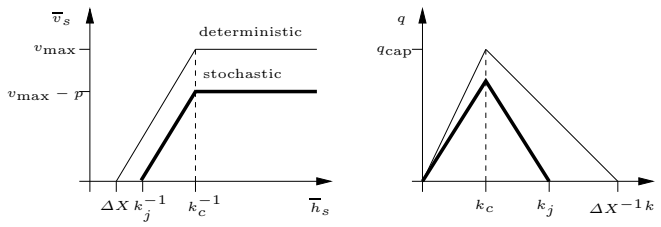

Fig. 4. *Left:* deriving a stationary $\overline{v}_{s_e}(\overline{h}_s)$ fundamental diagram from the STCA's constraints C1 – C9. The stochastic diagram has a higher inverse jam density, but the same inverse critical density as its deterministic counterpart (for the same v_{max}). *Right:* an equivalent triangular $q_e(k)$ fundamental diagram.

In conclusion, we note how rewriting the STCA's rule set allowed us to obtain a stationary triangular $q_e(k)$ fundamental diagram. This fundamental diagram, which implicitly incorporates the STCA's stochasticity, can then be specified as a parameter to the macroscopic first-order LWR model of section 2.3. Finally note that the shape of the derived fundamental diagram is dictated by the inequality constraints C1 – C9. As such, it actually represents an 'outer envelope', that is to say, all possible fundamental diagrams lie beneath this envelope. This includes curved fundamental diagrams, more generally piecewise linear fundamental diagrams, et cetera.

4 Application to an illustrative case study

After deriving a relation between the STCA and LWR models by means of the process explained in the previous section 3, we now apply our methodology to a small case study. We first describe the setup of the test scenario, after which we interpret and discuss our obtained results.

4.1 Description of the case study

The case study we consider, is modeled as a single-lane road that has a middle section with a reduced maximum speed (corresponding to e.g., an elevation, a speed limit, ...). This road consists of three consecutive segments A, B, and C, as depicted in Fig. 5, whereby vehicles enter the road at segment A, travel through segment B, and exit it at the end of segment C. For the STCA, we assume a temporal and spatial discretization of $\Delta T = 1$ s and $\Delta X = 7.5$ m, respectively. The first road segment A then consists of 1500 cells (11.25 km), while the second and third segments B and C each consist of 750 cells (i.e., each approximately 5.6 km long). The maximum speed for segments A and C is $v_{\text{max}}^{A,C} = 5$ cells/time step, whereas it is $v_{\text{max}}^{B} = 1$ cell/time step for segment B. The capacity flows for all three segments are denoted as $q_{\text{cap}}^{A,C}$ and q_{cap}^{B}.

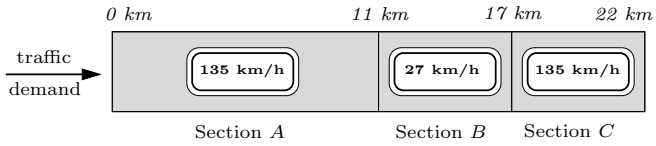

Fig. 5. The single-lane road of the case study we consider, consisting of three consecutive segments A, B, and C. Assuming temporal and spatial discretizations of $\Delta T = 1$ s and $\Delta X = 7.5$ m, respectively, segment A is composed of 1500 cells, while segments B and C are each composed of 750 cells. The maximum speed for segments A and C is $v_{\text{max}} = 5$ cells/time step, whereas it is $v_{\text{max}} = 1$ cell/time step for segment B.

This road is simulated using both the STCA and the LWR model, each time for 3000 time steps. As for the boundary conditions, we assume an overall inflow of $q_{\text{cap}}^{B}/2$, except from time step 200 until time step 600, where we have created a short *traffic burst* of increased demand, with an inflow of $(q_{\text{cap}}^{A,C} + q_{\text{cap}}^{B})/2$. Fig. 6 shows a close up of the individual vehicle trajectories for the STCA in a time-space diagram, near the border between segments A and B. As can be seen from the trajectories, heavy congestion sets in and flows upstream into segment A, where it starts to dissolve at the end of the traffic burst. The result is a typical triangular-shaped region that contains a queue of slow-moving vehicles (the backward propagating waves are clearly distinguished as the pattern of parallel black and white stripes).

Applying our previously discussed methodology, we construct a stationary triangular $q_e(k)$ fundamental diagram. Its parameters are calculated by means of equations (20) – (23). The results are listed in Table 1, with the TCA's parameters expressed in cells/time step, vehicles/cell, and vehicles/time step, respectively, and the LWR's parameters expressed in kilometres/hour, vehicles/-kilometre, and vehicles/hour, respectively.

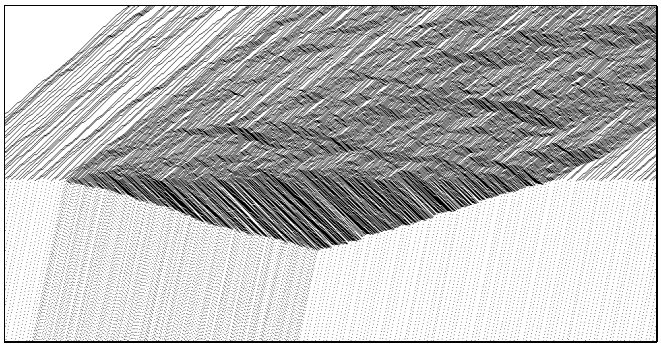

Fig. 6. A close up of the individual vehicle trajectories for the STCA in a time-space diagram, near the border between segments A ($v_{\max}^{A,C} = 5$ cells/time step) and B ($v_{\max}^{B} = 1$ cell/time step), for $p = 0.1$ everywhere in the system. We can see the formation and dissolution of an upstream growing congested region at the end of segment A, related to the short traffic burst.

$v_{\max} = 1 \quad (p = 0.1)$			$v_{\max} = 5 \quad (p = 0.1)$		
	TCA	LWR		TCA	LWR
$\overline{v}_{\text{ff}}$	0.90	24.30	$\overline{v}_{\text{ff}}$	4.90	132.30
k_{crit}	0.50	66.67	k_{crit}	0.17	22.22
k_{jam}	0.91	121.20	k_{jam}	0.91	121.20
q_{cap}	0.45	1620.08	q_{cap}	0.83	2939.71

$v_{\max} = 1 \quad (p = 0.5)$			$v_{\max} = 5 \quad (p = 0.5)$		
	TCA	LWR		TCA	LWR
$\overline{v}_{\text{ff}}$	0.50	13.50	$\overline{v}_{\text{ff}}$	4.50	121.50
k_{crit}	0.50	66.67	k_{crit}	0.17	22.22
k_{jam}	0.67	88.89	k_{jam}	0.67	88.89
q_{cap}	0.25	900.05	q_{cap}	0.77	2699.73

Table 1. The resulting parameters for the triangular fundamental diagrams, as calculated by means of equations (20) – (23). The TCA's parameters are expressed in cells/time step, vehicles/cell, and vehicles/time step, respectively, whereas the LWR's parameters are expressed in kilometres/hour, vehicles/kilometre, and vehicles/hour, respectively.

4.2 Results and discussion

The result of numerically solving the LWR model for the case of $p = 0.1$ using the Godunov method [2,9], is depicted in the right part of Fig. 7. Note that for the LWR model, each cell in the Godunov scheme corresponds to 5 (i.e., $v_{\max}^{A,C}$) consecutive cells of the STCA model. Comparing the tempo-spatial behavior of the LWR model to that of the microscopic system dynamics of the STCA model (i.e., the left part of Fig. 7), we find a good *qualitative* agreement between the two approaches. With respect to the first-order traffic flow characteristics, we note that the buildup and dissolution of congestion queues are fairly analogous for both techniques.

In Fig. 8, we show the results when repeating the same experiment, but this time with the stochastic noise p set to 0.5 for all three segments. As revealed by the shape of the dark triangular region in the LWR model (right part), the buildup and dissolution of congestion queues seems to be *exaggerated*, especially in the upstream flowing queue of segment A.

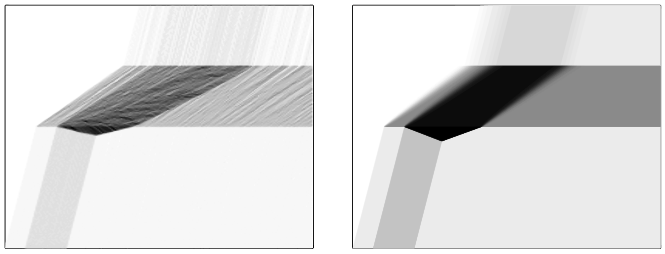

Fig. 7. Time-space diagrams showing the propagation of densities during 3000 time steps for the road in the case study. *Left:* the microscopic system dynamics of the STCA model. *Right:* the results for the LWR model. In both cases, $p = 0.1$, with darker regions corresponding to more congested traffic conditions. There is a qualitatively good agreement between the two approaches on the level of first-order traffic flow characteristics: the buildup and dissolution of congestion queues are fairly analogous for both techniques.

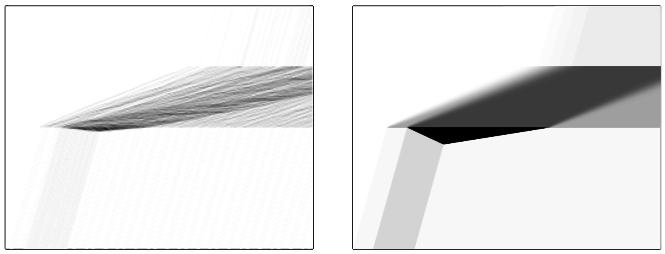

Fig. 8. Time-space diagrams showing the propagation of densities during 3000 time steps for the road in the case study. *Left:* the microscopic system dynamics of the STCA model. *Right:* the results for the LWR model. In both cases, $p = 0.5$, with darker regions corresponding to more congested traffic conditions. As revealed by the shape of the dark triangular region in the LWR model (right part), the buildup and dissolution of congestion queues is exaggerated, especially in the upstream flowing queue of segment A.

It is interesting to note that the STCA model reveals a *higher-order effect* that is not visible in the LWR model: there exists a fan of forward propagating density waves in segment B (see the left parts of Fig. 7 and Fig. 8). As such, in its tempo-spatial diagram, the STCA seems to be able to visualize the characteristics that constitute the solution of the LWR model.

In order to more rigourously quantify the discrepancies between the time-space diagrams of both STCA and LWR models, we provide their *absolute differences* in Fig. 9. The left part shows the differences for $p = 0.1$, whereas the right part shows the differences for $p = 0.5$. The most important features to look at, are the dark colored regions which indicate larger differences between both modeling approaches. We can clearly see that there is a problem with respect to a *quantitative* agreement between both STCA and LWR models. It appears as though the LWR model *overestimates* the STCA's capacity flows. As a re-

sult, it dissolves its jams more quickly in segment B, and it predicts a more severe onset of congestion in segment A (i.e., the triangular-shaped region containing the spill-back queue is more pronounced in the LWR's case). The sharply pronounced darker regions in the tempo-spatial left part of segment B, are due to the fact that the LWR model does not visualize the characteristics of its solution, in contrast to the STCA model which is able to give a clear indication of them.

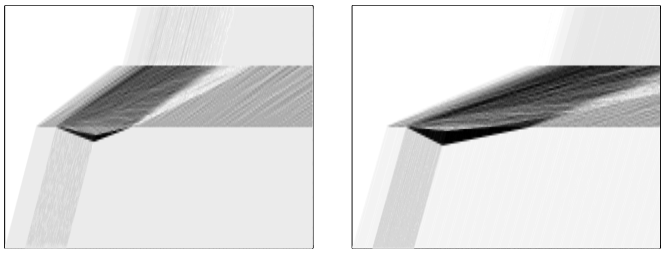

Fig. 9. Time-space diagrams showing the differences in densities for the STCA and LWR models, during 3000 time steps for the road in the case study. Darker regions indicate large differences between both modeling approaches. *Left:* the differences for $p = 0.1$ are less pronounced, showing only a dark edge at the bottom triangular-shaped region in segment A. *Right:* the differences for $p = 0.5$, showing significant discrepancies in the bottom of the triangular-shaped region in segment A.

One of the main reasons for this discrepancy between both modeling approaches, lies in the derivation of a triangular $q_e(k)$ fundamental diagram for the LWR model, as was explained in section 3. Because we assumed a stationarity condition on the STCA's rule set, the resulting constraints implied an invariant critical density, and always overestimated the STCA's capacity flows. In our opinion, the different behavior of both models, mainly stems from this artifact. As a result, the discrepancies will become more articulated when increasing the stochastic noise p.

5 Alternate derivation of the fundamental diagram

Considering the results of the previous approach, i.e., deriving the LWR's fundamental diagram based on the STCA's rule set, and the problems related to it, the next step is to specify the fundamental diagram *directly*, based on the empirically observed behavior of the STCA model. In the following two sections, we first discuss the effects of explicitly adding noise to the LWR's fundamental diagram, after which we discuss our obtained results when specifying the fundamental diagram directly.

5.1 The effect of adding noise to the LWR's fundamental diagram

Adding noise to the LWR model can mainly be accomplished via two ways: either by explicitly incorporating noise terms in the LWR equations (e.g., the conservation equation), or as a noise term in the $q_e(k)$ relation (i.e., the fundamental diagram). We refrain from changing the LWR's conservation equation, because this amounts to introducing some form of numerical diffusion, similar to the viscosity terms that are originally encountered in the conservation equation's (6) right-hand side (which we set to zero in order to obtain the inviscid LWR model).

In Fig. 10, we show the results of supplying uniformly distributed additive noise of 0.1 (left part) and 0.5 (right part). As can be seen, the introduction of noise in the fundamental diagram, leads to a 'spreading' of the solution. For small noise levels, some of the characteristics are revealed; for larger noise levels, the characteristics are clearly pronounced, including long jam dissolution times.

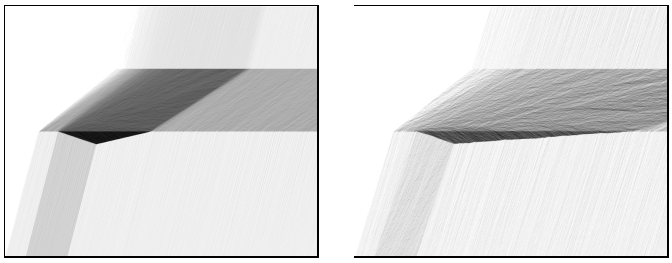

Fig. 10. Time-space diagrams showing the propagation of densities during 3000 time steps for the road in the case study. Depicted are the results for the LWR model, with noise levels of 0.1 (*left*) and 0.5 (*right*). Higher noise levels clearly reveal the typical characteristics of the solution, and introduce longer jam dissolution times.

5.2 Specifying the fundamental diagram directly

Instead of deriving the fundamental diagram based on the approach taken in section 3, we now try to obtain the values for the critical densities and capacity flows directly, by looking at the STCA's (k,q) diagrams in Fig. 11 (an equivalent procedure would be to measure the capacity flows directly from the time-space diagram in Fig. 6). Considering the STCA's (k,q) diagrams in Fig. 11, we can estimate its capacities at approximately $q^B_{\text{cap}} = 0.34$ vehicles/time step ≈ 1220 vehicles/hour, and $q^{A,C}_{\text{cap}} = 0.67$ vehicles/time step ≈ 2400 vehicles/hour for $v^B_{\text{max}} = 1$ and $v^{A,C}_{\text{max}} = 5$ cells/time step, respectively. The stochastic noise p was set to 0.1 for all three segments. Changing p to 0.5 for these segments, we can estimate the capacities at approximately $q^B_{\text{cap}} = 0.15$ vehicles/time step ≈ 540 vehicles/hour, and $q^{A,C}_{\text{cap}} = 0.34$ vehicles/time step ≈ 1220 vehicles/hour for $v_{\text{max}} = 1$ and $v_{\text{max}} = 5$ cells/time step, respectively.

Instead of calculating the capacity flows from the average free-flow speeds and the critical densities, as was done by means of equation (23), we now specify these capacity flows directly to the LWR's fundamental diagrams and calculate the critical densities from them. The results we obtained, are visualized in the time-space diagrams

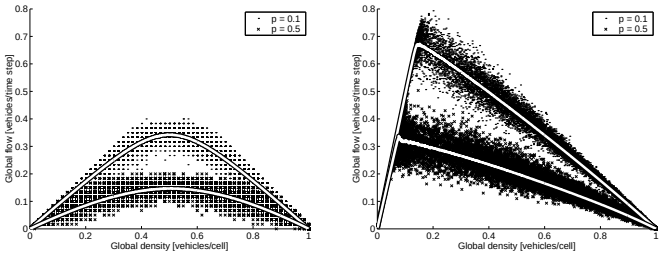

Fig. 11. The (k,q) fundamental diagrams for the STCA model. *Left:* two diagrams for $v_{\max}^{B} = 1$ cells/time step. *Right:* two diagrams for $v_{\max}^{A,C} = 5$ cells/time step. Each time, the slowdown probability $p \in \{0.1, 0.5\}$. Note how a slower maximum speed makes the diagrams more curved, and how an increasing slowdown probability leads to both a lower critical density and capacity flow.

of Fig. 12. Because the STCA's capacity flows are now better approximated, and not overestimated as with the previous methodology, there seems to be a better qualitative agreement for both noise levels with the STCA's time-space diagrams in the left parts of Fig. 7 and Fig. 8.

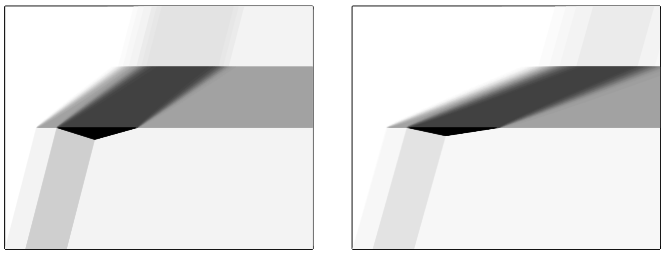

Fig. 12. Time-space diagrams showing the propagation of densities during 3000 time steps for the road in the case study. *Left:* the results for the LWR model with $p = 0.1$. *Right:* the results for the LWR model with $p = 0.5$. In both diagrams, the fundamental diagram was specified directly to the LWR model, by explicitly stipulating the capacity flows of the STCA model. As a result, there seems to be a better qualitative agreement for both noise levels with the STCA's time-space diagrams in the left parts of Fig. 7 and Fig. 8.

In Fig. 13 we have depicted the absolute differences between this approach and the STCA's time-space diagrams. Comparing this to the previous results of Fig. 9, we can see that in both cases the buildup and dissolution of congestion queues is in good qualitative agreement for both noise levels. *As such, we come the conclusion that it is vital to correctly capture the capacity flows of the STCA model.* Neglecting this property, can result in severe distortion of the system dynamics for higher noise levels.

Note that the LWR model is able to correctly capture the first-order effects of jam buildup and dissolution, and that, due to its microscopic treatment, the STCA model allows us to visualize the higher-order effects inside jam. However, as is evidenced by this and the previous section, it is very important to correctly capture the capacity flows in the STCA model, otherwise a growing discrepancy between the LWR and STCA model is introduced with higher noise levels.

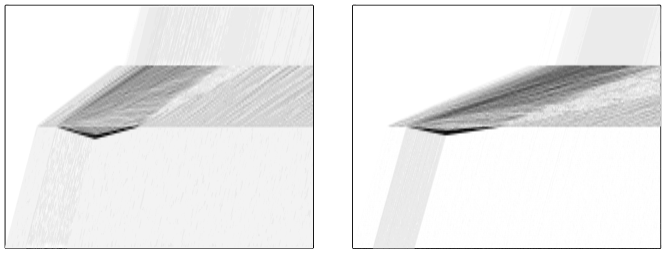

Fig. 13. Time-space diagrams showing the differences in densities for the STCA and LWR models, during 3000 time steps for the road in the case study. Darker regions indicate large differences between both modeling approaches. *Left:* the differences for $p = 0.1$. *Right:* the differences for $p = 0.5$. In both cases, the differences are less pronounced, showing only dark edges at the bottom of the triangular-shaped region in segment A.

6 Conclusions

In this paper, we presented an alternate methodology for implicitly incorporating the STCA's stochasticity into the macroscopic first-order LWR model. The innovative aspect of our approach, is that we derive the LWR's fundamental diagram directly from the STCA's rule set, by assuming a stationarity condition that converts the STCA's rules into a set of linear inequalities. In turn, these constraints define the shape of the fundamental diagram that is then specified to the LWR model.

For noise-free systems, our method is exact. In the presence of noise, however, the capacity flows in the derived fundamental diagram are overestimates of those of the STCA model. This discrepancy can be explained as follows: the underlying assumption for the LWR model, is that the fundamental diagram is assumed to be exact, and implicitly obeyed, i.e., the existing equilibrium relation is representative for the real traffic situation. In the original LWR formulation, this relation was also assumed to hold also for non-stationary traffic (which is a more or less reasonable assumption if we consider long and crowded roads). Our calculations have shown that a direct translation of the STCA's rule set into the LWR's fundamental diagram, does not always result in a valid fundamental diagram, especially for higher noise levels. As such, there can be a significant difference between an *average* fundamental diagram (STCA) and a *stationary* fundamental diagram (LWR). As a result, the STCA model is able to temporarily operate under larger flows and densities than those possible for the LWR's stationary fundamental diagram. A logical course of action would to better approximate the STCA's fundamental diagram. By doing so however, we lose the advantage gained through an explicit derivation of the fundamental diagrams' outer envelope, almost certainly leading to extra conditions that need to make further assumptions about its shape. Directly specifying the

STCA's capacity flows to the triangular LWR fundamental diagram, effectively remedies most of the mismatches between both STCA and LWR models.

Our methodology sees the STCA complementary to the LWR model and vice versa, so the results can be of great assistance when interpreting the traffic dynamics in both models. Especially appealing, is the fact that the STCA can visualise the higher-order characteristics of traffic stream dynamics, e.g., the fans of rarefaction waves. Nevertheless, because the LWR model is only a coarse representation of reality, there are still some mismatches between the two approaches. One of the main concerns the authors discovered, is as hinted at earlier, the fact that using a stationary fundamental diagram (i.e., an equilibrium relation between density and flow), always overestimates the practical capacity of a stochastic cellular automaton model. As such, it is vital to correctly capture the capacity flows in both STCA and LWR models, a remark that we feel is valid for all case studies.

Acknowledgements

Dr. Bart De Moor is a full professor at the Katholieke Universiteit Leuven, Belgium. Our research is supported by: **Research Council KUL**: GOA AMBioRICS, several PhD/postdoc & fellow grants, **Flemish Government**: **FWO**: PhD/postdoc grants, projects, G.0407.02 (support vector machines), G.0197.02 (power islands), G.0141.03 (identification and cryptography), G.0491.03 (control for intensive care glycemia), G.0120.03 (QIT), G.0452.04 (new quantum algorithms), G.0499.04 (statistics), G.0211.05 (Nonlinear), research communities (ICCoS, ANMMM, MLDM), **IWT**: PhD Grants, GBOU (McKnow), **Belgian Federal Science Policy Office**: IUAP P5/22 ('Dynamical Systems and Control: Computation, Identification and Modelling', 2002-2006), PODO-II (CP/40: TMS and Sustainability), **EU**: FP5-Quprodis, ERNSI, **Contract Research/agreements**: ISMC/IPCOS, Data4s,TML, Elia, LMS, Mastercard.

References

1. Debashish Chowdhury, Ludger Santen, and Andreas Schadschneider. Statistical physics of vehicular traffic and some related systems. *Physics Reports*, 329:199–329, 2000.
2. Carlos F. Daganzo. A finite difference approximation of the kinematic wave model of traffic flow. *Transportation Research B*, 29B(4):261–276, 1995.
3. Carlos F. Daganzo. *Fundamentals of Transportation and Traffic Operations*. Elsevier Science Ltd., 2 edition, 1997. ISBN 0-08-042785-5.
4. B. Derrida, E. Domany, and D. Mukamel. An exact solution of a one-dimensional asymmetric exclusion model with open boundaries. *Journal of Statistical Physics*, 69:667–687, 1992.
5. Nathan Gartner, Hani Mahmassani, Carroll J. Messer, Henry Lieu, Richard Cunard, and Ajay K. Rathi. *Traffic Flow Theory: A State-of-the-Art Report*. Technical report, Transportation Research Board, December 1997.
6. F.A. Haight. *Mathematical theories of traffic flow*. New York Academic Press, 1963.
7. Ansgar Jüngel. *Modeling and Numerical Approximation of Traffic Flow Problems*. Universität Mainz, December 2002.
8. S. Krauß, Kai Nagel, and Peter Wagner. The mechanism of flow breakdown in traffic flow models. In *Proceedings of the International Symposium on Traffic and Transportation Theory (ISTTT99)*, Jerusalem, 1999.
9. J.P. Lebacque. The Godunov scheme and what it means for first order traffic flow models. In J.B. Lesort, editor, *Proceedings of the 13th International Symposium on Transportation and Traffic Theory (ISTTT)*. Pergamon, Oxford, November 1996.
10. M.J. Lighthill and G.B. Whitham. On kinematic waves: II. A theory of traffic flow on long crowded roads. In *Proceedings of the Royal Society*, volume A229, pages 317–345, 1955.
11. Sven Maerivoet. *Cellular automata models of road traffic – Analytical results*, chapter 4 (PhD thesis), pages 198–200. Katholieke Universiteit Leuven, 2005.
12. Sven Maerivoet, Steven Logghe, Bart De Moor, and Ben Immers. A comparison of a cellular automaton and a macroscopic model. In M. Schreckenberg, editor, *Proceedings of the Workshop on Traffic and Granular Flow '03*, Delft, The Netherlands, October 2003. Delft University of Technology.
13. Kai Nagel. Life-times of simulated traffic jams. *International Journal of Modern Physics C*, 5(3):567–580, 1994.
14. Kai Nagel. *High-speed microsimulations of traffic flow*. PhD thesis, Universität zu Köln, March 1995.
15. Kai Nagel. Particle hopping models and traffic flow theory. *Physical Review E*, 53(5):4655–4672, May 1996.
16. Kai Nagel and Michael Schreckenberg. A cellular automaton model for freeway traffic. *Journal de Physique I France*, 2:2221–2229, 1992.
17. Kai Nagel, Peter Wagner, and Richard Woesler. Still flowing: old and new approaches for traffic flow modeling. *Operations Research*, 51(5):681–710, 2003.
18. L.A. Pipes. Hydrodynamic approaches. In D.L. Gerlough and D.G. Capelle, editors, *An Introduction to Traffic Flow Theory*, Washington, D.C., 1964. Highway Research Board. Special Report 79.
19. Paul I. Richards. Shockwaves on the highway. *Operations Research*, 4:42–51, 1956.
20. Ludger Santen. *Numerical Investigations of Discrete Models for Traffic Flow*. PhD thesis, Universität zu Köln, 1999.
21. Andreas Schadschneider. The Nagel-Schreckenberg model revisited. *European Physical Journal B*, 10(3):573–582, August 1999.
22. Andreas Schadschneider. Traffic flow: A statistical physics point of view. *Physica A*, 313:153–187, 2002.
23. Andreas Schadschneider and Michael Schreckenberg. Car-oriented mean-field theory for traffic flow models. *Journal of Physics A*, 30:69–75, 1997.
24. Andreas Schadschneider and Michael Schreckenberg. Garden of Eden states in traffic models. *Journal of Physics A*, 31:225–231, 1998.
25. M. Schreckenberg, A. Schadschneider, K. Nagel, and N. Ito. Discrete stochastic models for traffic flow. *Physical Review E*, 51(4):2939–2949, April 1995.
26. J.G. Wardrop. Some theoretical aspects of road traffic research. In *Proceedings of the Institution of Civil Engineers*, volume 1 of *2*, 1952.